

## Regular Article

# Visible and near-infrared luminescent properties of Pr<sup>3+</sup> doped strontium molybdate thin films by a facile polymer-assisted deposition process



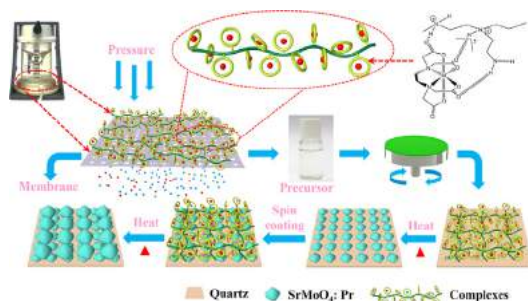
Fengjun Chun<sup>a</sup>, Wen Li<sup>a</sup>, Binbin Zhang<sup>a</sup>, Wen Deng<sup>a</sup>, Xiang Chu<sup>a</sup>, Hai Su<sup>a</sup>, Hanan Osman<sup>a</sup>, Haitao Zhang<sup>a</sup>, Xiaoyun Zhao<sup>b</sup>, Weiqing Yang<sup>a,c,\*</sup>

<sup>a</sup> Key Laboratory of Advanced Technologies of Materials (Ministry of Education), School of Materials Science and Engineering, China

<sup>b</sup> College of Optoelectronic Technology, Chengdu University of Information Technology, Chengdu 610225, China

<sup>c</sup> State Key Laboratory of Traction Power, Southwest Jiaotong University, Chengdu 610031, China

## GRAPHICAL ABSTRACT



## ARTICLE INFO

## Article history:

Received 12 May 2018

Revised 28 June 2018

Accepted 11 July 2018

Available online 19 July 2018

## Keywords:

SrMoO<sub>4</sub>:Pr

Multilayer thin films

Polymer-assisted deposition

Quartz substrate

Visible and NIR emission

## ABSTRACT

Quartz substrate supported Praseodymium (Pr) doped strontium molybdate (SrMoO<sub>4</sub>) thin films with good uniformity and outstanding fluorescent properties are successfully fabricated via a facile polymer-assisted deposition (PAD) method. In combination with the strong chelating effect of water-soluble polymer on metal cations, the free cations without chelating are effectively ruled out but the remaining chelating metal cations are employed for the highly uniform and accurate stoichiometry luminescent SrMoO<sub>4</sub>:Pr thin films, layer-by-layer mounting on the common quartz substrates. More importantly, the excellent release of stress from polymer during the growth process of epitaxial thin film can effectively overcome the mismatch between thin film and common quartz substrate and then guarantee the quality of thin film. Under the ultraviolet (UV) light excitation, the samples show high luminescence intensity both in visible and near-infrared (NIR) regions peaked at 646 nm and 1037 nm, mainly ascribing to the transitions of <sup>3</sup>P<sub>0</sub> → <sup>3</sup>F<sub>2</sub> and <sup>1</sup>G<sub>4</sub> → <sup>3</sup>H<sub>4</sub> of Pr<sup>3+</sup> ions. The luminescent properties can be tailored by optimizing the number of spin-coated layers and doping concentrations. The maximum emission occurs at 4 mol% of Pr<sup>3+</sup> dopant, and it exhibits an impressive high photoluminescence quantum yield (QY) of up to 86.12%. These results evidently demonstrate the present PAD method is a useful prototype for preparing high performance luminescent thin films even on the cheap quartz substrate.

© 2018 Elsevier Inc. All rights reserved.

## 1. Introduction

Recently, metal molybdates (RMOO<sub>4</sub>), emerged as promising host materials in phosphors industry, have received considerable

\* Corresponding author at: State Key Laboratory of Traction Power, Southwest Jiaotong University, Chengdu 610031, China.

E-mail address: [wqyang@swjtu.edu.cn](mailto:wqyang@swjtu.edu.cn) (W. Yang).

research attentions due to their high thermal and chemical stability, high light yield, high average refractive index and versatile potential applications [1–3]. Generally,  $\text{RMO}_4$  ( $R = \text{Ca}, \text{Ba}, \text{Sr}, \text{Pb}$ ) share the scheelite-type structure, and this kind of the unique crystal structure has been confirmed to possess more excellent optical performance than other crystal structures. As a promising alternative material used in white LEDs, every centrally located Mo atoms in molybdates ( $\text{RMO}_4$ ,  $R = \text{Sr}, \text{Ba}, \text{Ca}$  et al.) is coordinated by four O atoms to form the stable structure  $\text{MoO}_4^{2-}$ , which will absorb the external energy in the near ultraviolet (UV) and then transfer energy to rare earth ions [4,5]. It has been reported that the  $\text{RMO}_4$  have been doped feasibly by rare-earth metals, such as  $\text{Dy}^{3+}$ ,  $\text{Tb}^{3+}$ ,  $\text{Sm}^{3+}$ , and  $\text{Eu}^{3+}$ , which showed enhanced luminescent properties with broad and intense absorption bands due to the charge transfer [4,6]. Among the various molybdates,  $\text{SrMoO}_4$  possesses the unique advantages of low phonon energy, wide band gap, and stable structure, leading potential application in luminescence devices [7]. So, rare earth ions activated  $\text{SrMoO}_4$  phosphors are extensively investigated, indicating complicated energy level scheme and diverse optimal emission in various host materials. Dunaeva et al. [8] and Cao et al. [9] applied the Czochralski technique to grow a  $\text{Pr}^{3+}$ -doped  $\text{SrMoO}_4$  single crystal, and the heat conductivity and luminescence lifetime were improved by doping  $\text{Pr}^{3+}$  ions. In addition, Xia et al. used high-temperature solid-state reaction method to prepare  $\text{Pr}^{3+}$ ,  $\text{Yb}^{3+}$  and  $\text{Sm}^{3+}$  co-doped  $\text{SrMoO}_4$  phosphors [10]. These studies indicate an exciting phenomenon that a new near-infrared (NIR) emission around 1040 nm can be attributed to the  $^1\text{G}_4 \rightarrow ^3\text{H}_4$  transition of  $\text{Pr}^{3+}$  ions. NIR emission materials are closely relevant to widespread applications, such as bio-imaging, optical telecommunications, amplifiers, and waveguides [1,11–14]. However, the conventional fluorescent phosphors for white LEDs present the heat dissipation issues, and it is difficult to get the uniform white light. In contrast, the fluorescent thin films exhibit higher uniformity, better adhesion, higher resolution and superior thermal conductivity when they are applied in displays and sensors for stress and temperature, it is a desired form for the solid-state device [15,16]. Generally, the fluorescent thin films mostly synthesized via pulsed laser deposition, ion-beam evaporation, RF sputtering and laser ablation methods in which expensive equipment or complicated process are compulsory to hinder their further commercial applications [17–19]. Furthermore, the stronger interfacial stress caused by the mismatches between thin film and common substrate is still a great challenge to date. Hence, it is essential to seek for simple and convenient means to prepare high-quality fluorescent thin films. In our previous work, broccoli-like superparticles were prepared by a polymer-assisted hydrothermal method [20]. The metal ions bind to the water-soluble polymers to effectively control the nucleation and growth process, this render us some enlightenment to synthesize  $\text{SrMoO}_4$ :  $\text{Pr}^{3+}$  luminescent thin films.

Polymer-assisted deposition (PAD), firstly reported in 2004, acting as an aqueous chemical solution route is a simple and low-cost method for preparing high-quality metal epitaxial films such as single element materials, metal-oxides, metal-nitrides and metal-carbides [21–26]. PAD is proposed as an efficient method based on the chemical solution deposition, metal precursors and water-soluble polymer are main components, and the soluble polymer is used for binding with metal ions directly to control the nucleation and growth of highly crystalline epitaxial films [24,27]. The metal ions bonded by polymer can homogeneously distribute in the precursor polymeric solution, strongly prevent from attending in secondary chemical reaction and effectively control the growth stress of thin film mounted on the substrate [28]. Therefore, all above characteristics in PAD method are beneficial to prepare luminescent thin films with high quality. Furthermore,  $\text{Pr}^{3+}$ -doped  $\text{SrMoO}_4$  thin films have never been investigated, and all

the more so for the NIR luminescent emission of  $\text{Pr}^{3+}$  with various doping concentration.

In this paper,  $\text{Pr}^{3+}$ -doped  $\text{SrMoO}_4$  multilayer luminescent thin films with good uniformity and high luminescent properties are successfully prepared on the common quartz substrate via the PAD method for the first time. The samples show high luminescence properties both in visible and NIR regions peaked at 646 nm and 1037 nm by the UV light excitation, and the thin films show exciting high photoluminescence quantum yield. These promising results obtained strongly suggest that the PAD method is a lighthouse for preparing high-performance luminescent thin films, even on low-cost common quartz substrate.

## 2. Experimental section

### 2.1. Preparation of precursor solution

In this present work, the raw materials were EDTA (Aldrich), PEI (99.99%, Aladdin),  $\text{Sr}(\text{NO}_3)_2$  (AR, Keshi),  $(\text{NH}_4)_6\text{Mo}_7\text{O}_{24}\cdot 4\text{H}_2\text{O}$  (AR, Keshi), and  $\text{PrCl}_3\cdot 6\text{H}_2\text{O}$  (99.99%, Aladdin). First, 1 g EDTA and 1 g PEI were dissolved in 40 mL deionized water. After that,  $\text{Sr}(\text{NO}_3)_2$  were added to the former solution bit by bit with continuous stirring for 1 h at the room temperature. Then Amicon filtration was used at least 3 times to filtrate the solution, the filtrated solution was labeled as A. The solutions contain  $\text{Mo}^{2+}$  and  $\text{Pr}^{3+}$  are prepared with the same method, and these two solutions were labeled as B and C, respectively. The ultimate concentration of  $\text{Sr}^{2+}$ ,  $\text{Mo}^{6+}$  and  $\text{Pr}^{3+}$  in the A, B and C solutions can be confirmed by inductively coupled plasma atomic emission spectroscopy (ICP-AES). The actual concentration of  $\text{Sr}^{2+}$ ,  $\text{Mo}^{6+}$  and  $\text{Pr}^{3+}$  ions are 7.46 mg/mL, 15.7 mg/mL and 13.55 mg/mL, respectively. Finally, the precursor solutions of  $\text{SrMoO}_4$ :  $\text{Pr}_c$  ( $c = 0.01\text{--}0.06$ ) were obtained by mixing the filtrated solution of  $\text{Sr}^{2+}$ ,  $\text{Mo}^{6+}$ , and  $\text{Pr}^{3+}$  ions with a desired molar ratio.

### 2.2. The growth of $\text{SrMoO}_4$ : $\text{Pr}$ thin films

Quartz substrates were cleaned several times with acetone and ethanol prior to deposition. The as-prepared precursor solution was spin-coated on quartz substrates at 600 rpm for 10 s and 3000 rpm for 20 s. Soft-baking on a hot plate at 100 °C in air for 10 min was required to remove the residual water. Finally, the precursor thin film was thermal treated in a muffle furnace. It was heated to 510 °C with a low ramp rate of 1 °C/min and dwelled for 2 h to make sure the thermal decomposition of PEI and EDTA. Then the samples were heated at a high ramp rate of 10 °C/min from 500 °C to 800 °C, after annealing for 30 min, the thin films were cooled down to 200 °C with the speed of 2 °C/min. The spin-coating and thermal treatment processes were repeated multiple times depending on the designed film thickness. Finally, high-quality luminescent thin films were obtained when the films were cooled down to the room temperature.

### 2.3. Characterization

The crystal structure and phase composition of  $\text{Pr}^{3+}$ -doped  $\text{SrMoO}_4$  thin films were identified by the X'Pert Pro (Holland) X-ray diffract meter with  $\text{Cu K}\alpha_1$  radiation ( $\lambda = 0.15406$  nm). SEM images of samples were examined using scanning electron microscopy (SEM, S4800). The photoluminescence and photoluminescence excitation spectra were investigated at room temperature using FLS980 (Edinburgh Instruments) spectrometer with a 450 W Xenon lamp. Their photoluminescence quantum yields were analyzed using the absolute photoluminescence quantum yield measurement system that came with FLS980 (Edinburgh

Instruments). Decay times were measured under excitation at 265 nm with a 60 W microsecond pulsed Xenon flash lamp at room temperature (FLS980).

### 3. Result and discussion

In the PAD process, the homogeneous distribution of metal ions in the precursor solution is a crucial factor for obtaining high-quality thin films. Fig. 1a is a schematic illustration of the filtration step demonstrating a visual separation process between the metal ions bonded with the polymer via electrostatic attraction, hydrogen bonding and/or covalent bonding and the unbound ones [24,27]. In our work, metal ions coordinated with EDTA can form stable complexes which were abstractly displayed as light green circle with an internal ball. Then, the complexes bind to high molecular weight PEI (up to 25,000 Da), and the deep green chains were employed to denote PEI. Subsequently, the final mixed solution was purified by Amicon ultrafiltration containing a PM 10 ultrafiltration membrane as shown in the inset of Fig. 1a. In the view of the low molecular weight and size of the unbound cations, the Amicon ultrafiltration was designed to remove non-coordinated ions species under pressure of the  $N_2$  gas, and the filtered precursor solution was reserved for further use. The precursor solution consisted of  $Sr^{2+}$ ,  $Mo^{6+}$  and  $Pr^{3+}$  was obtained after mixing the filtrated solution with a desired molar ratio.

The schematic illustration of the growth process of  $SrMoO_4$ : Pr thin film is shown in Fig. 1b. Firstly, the prepared precursor solution was spin-coated onto the quartz substrate, then the followed thermal treatment under oxygen atmosphere is beneficial to evaporate the water and completely burn up the bound polymer. After that, the polymer-free thin film was uniformly distributed on the substrate via the heterogeneous nucleation and the film is composed of many nanoparticles. To get a thin film with a desired thickness, the spin-coating and thermal treatment processes were repeated several times under precisely the same condition.

The crystal structure of  $SrMoO_4$  and  $Pr^{3+}$ -doped  $SrMoO_4$  thin film have been investigated by XRD, and the corresponding results are shown in Fig. 2a. Comparing with diffraction patterns of the three samples, the existence of a broad peak can be assigned to the quartz substrate. The diffraction peaks of  $SrMoO_4$  thin film are in good agreement with the standard data (JCPDS 08-0482). Moreover, the diffraction patterns of the  $Pr^{3+}$  doped  $SrMoO_4$  thin film well match with the undoped sample and no impurity phase is discovered, which implies that the crystal structure of  $SrMoO_4$  is remained after the incorporation of  $Pr^{3+}$ . Meanwhile, the  $Pr^{3+}$  should occupy the  $Sr^{2+}$  site in line due to the ionic radii of  $Pr^{3+}$  (about 0.1013 nm) is close with  $Sr^{2+}$  (approximately 0.112 nm) [29]. As we have seen, the diffraction peaks of the samples are sharp and the half peak width is narrow, indicating that the prepared thin films have high crystallinity. The crystal structure of  $SrMoO_4$ , which belongs to the scheelite-type structure with space group  $I4_1/a$ , is illustrated in Fig. 2b [3,4]. Each Mo atom is coordinated to four equivalent O atoms which results in  $MoO_4^{2-}$  tetrahedral symmetry configuration. The primary crystal lattice structure of  $SrMoO_4$  can be maintained when a handful of Sr ions are substituted by Pr ions due to the excellent stability of  $MoO_4^{2-}$  [3].

Various surface morphologies of  $SrMoO_4$ : Pr thin films with different layers are shown in Fig. 3. A distinct morphological conversion takes place from uniform small grains for the single-layer sample to the large grains for multilayer sample. Fig. 3a1, a2 display the surface micrographs of the  $SrMoO_4$ : Pr thin film with a single layer, and the smooth surface is composed of uniform and compact  $SrMoO_4$ : Pr tiny grains with a size of about 50 nm. When the  $SrMoO_4$ : Pr thin film has two layers formed by spin-coating, the grains size partly become larger, as shown in Fig. 3b1, b2. More large grains can be found intuitively when the number of layers increases to three, as shown in Fig. 3c1, c2. The particles of the upper layer are homogeneous with a particle size of  $\sim 200$  nm when the film comprises five layers, as illustrated in Fig. 3d1, d2. The corresponding image (Fig. 3e1, e2) of the eight-layer thin film

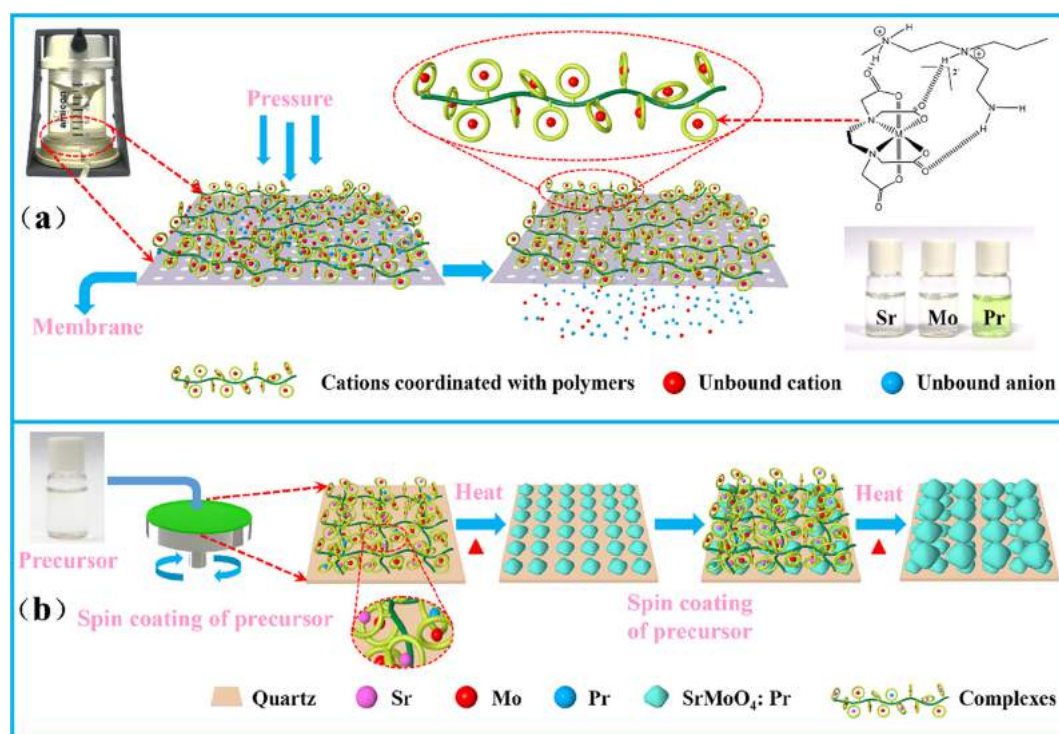


Fig. 1. Schematic illustration of PAD process. (a) The filtration process of accurately stoichiometry metal ions precursor coordinated with polymers. (b) The growth process of  $SrMoO_4$ : Pr thin film.

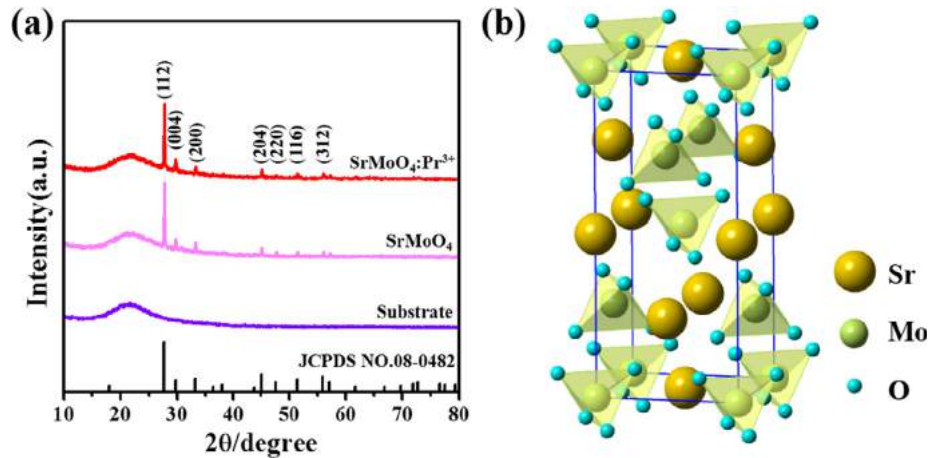


Fig. 2. The crystal characteristic of as-grown thin films. (a) XRD patterns of a quartz substrate, SrMoO<sub>4</sub> thin film and SrMoO<sub>4</sub>:Pr thin film. (b) Schematic crystal structures of SrMoO<sub>4</sub>.

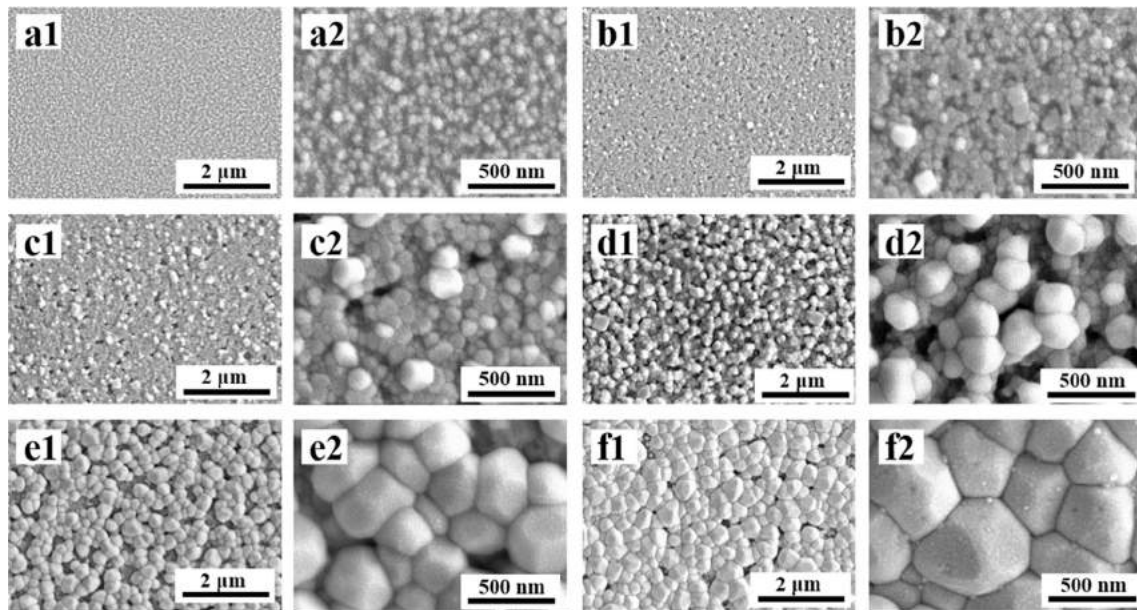


Fig. 3. Various enlarged surface SEM micrographs of the SrMoO<sub>4</sub>:Pr films with different layers: 1 layer (a1, a2), 2 layers (b1, b2), 3 layers (c1, c2), 5 layers (d1, d2), 8 layers (e1, e2), 12 layers (f1, f2).

consisted of larger nanoparticles and the size of the nanoparticles is ranging from 200 nm to 300 nm. As shown in Fig. 3f1, f2, thin film is rather dense and the grains further grow when the number of layers increases to twelve. The corresponding thin film evidently presents the perfect grains thin film due to mutual compression between the grains. This indicated that the grain growth is closely related to the number of spin-coated layers.

Cross-sectional SEM images of SrMoO<sub>4</sub>:Pr thin films with various layers are employed to further verify the relationship between the grains growth and the layers of thin film, as presented in Fig. 4. The thicknesses of selective five-, eight- and twelve-layers thin films were about 220 nm, 300 nm and 400 nm, respectively. The thickness of thin films range from 220 nm to 400 nm, while the number of layers varies from five to twelve, further verifying the growth mechanism of SrMoO<sub>4</sub>:Pr thin film originated from nanoparticles. More importantly, it is evident that the thin film tightly mounted on the common and low cost polycrystal quartz substrate. As we know, the previously reported high crystalline thin films were grown on the extra-expensive single crystal sub-

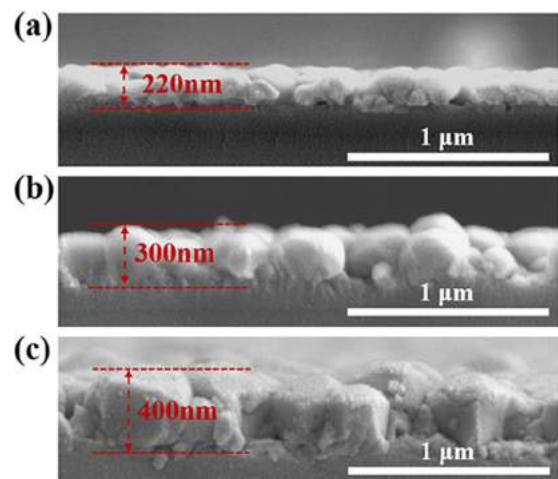
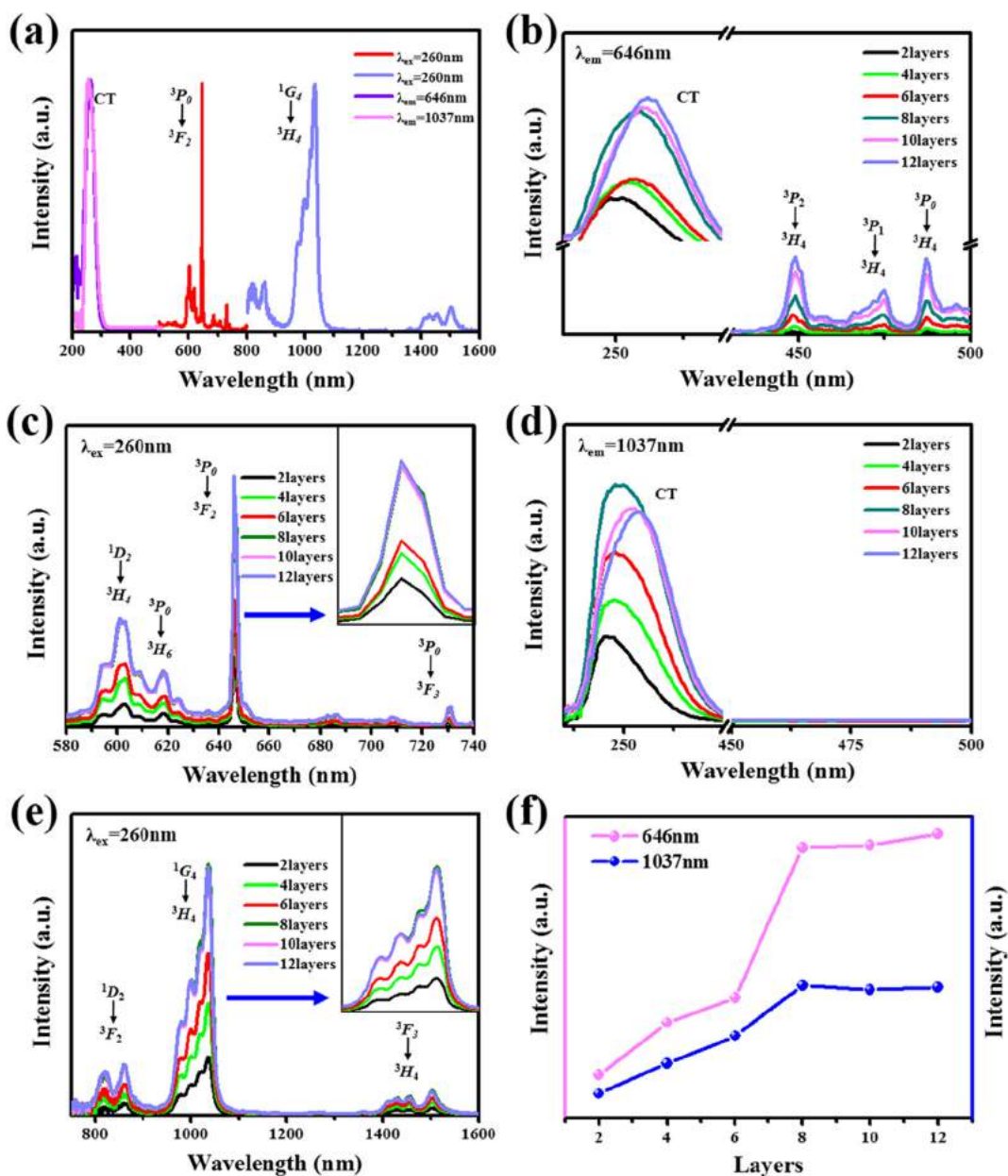


Fig. 4. Cross-sectional SEM images of SrMoO<sub>4</sub>:Pr thin films with various layers: 5 layers (a), 8 layers (b), 12 layers (c).

strates such as yttria-stabilized zirconia (YSZ), sapphire and  $\text{LaAlO}_3$  (LAO) [30–32]. It is more difficult to grow high-quality thin films on the common quartz substrate with polycrystal structures because of their more serious lattice mismatches leading to significant interfacial strain. However, in this work, the stronger chelating action of water-soluble polymer to metal could efficiently and slowly release interfacial strain during annealing of  $\text{SrMoO}_4:\text{Pr}$  thin film. The strain release process facilitates the mounting of the thin film on a normal quartz substrate [33]. Moreover, our layer-by-layer method can efficiently prevent the formation of microcracks and the stress of thin films may be minimized [34]. Therefore, this PAD method is evidently proved to be a potential growth process of high-quality complex metal-oxide films.

Fig. 5 describes the luminescent properties of  $\text{SrMoO}_4:\text{Pr}_{0.04}$  thin films with various layers in the visible and NIR regions. The

normalized photoluminescence spectra of  $\text{SrMoO}_4:\text{Pr}_{0.04}$  thin film in the visible and NIR regions are shown in Fig. 5a. The relative intensity of the visible emission spectra and NIR emission spectra can't be compared directly because the different detectors were employed to record the spectra. The excitation spectrum which is determined with an emission wavelength of 646 nm almost coincides with the spectrum monitored at 1037 nm, and the excitation peak located at 260 nm is attributed to the charge transfer. The excitation spectra of  $\text{SrMoO}_4$  thin films are monitored at 646 nm consisting of a broad excitation band and three weak peaks except for the different intensity, as illustrated in Fig. 5b. The broad band ranged from 230 nm to 270 nm can be attributed to the charge transfer (CT) transition in the  $\text{MoO}_4^{2-}$  groups from the oxygen ligands to the central molybdenum atom. The strong absorption of  $\text{MoO}_4^{2-}$  groups suggests the energy transfer from the matrix to



**Fig. 5.** The photoluminescence spectra of as-grown thin films. (a) The normalized photoluminescence excitation and emission spectra of  $\text{SrMoO}_4:\text{Pr}_{0.04}$  thin films. The excitation (b) and emission (c) spectra of  $\text{SrMoO}_4:\text{Pr}_{0.04}$  (2–12layers) thin films with emission wavelength at 646 nm and excitation wavelength at 265 nm. The excitation (d) and NIR emission (e) spectra of  $\text{SrMoO}_4:\text{Pr}_{0.04}$  thin films with emission wavelength at 1037 nm and excitation wavelength at 265 nm. (f) Visible and NIR integrated emission intensity of  $\text{SrMoO}_4:\text{Pr}_{0.04}$  thin films with various layers.

the activator ions [5]. As the number of layers increases, there is a red-shifted broad ultraviolet absorption, whereas the other three peaks in the visible regions are fixed. These three weak peaks centered at 450 nm, 476 nm and 487 nm corresponding to the transitions of  ${}^3P_2 \rightarrow {}^3H_4$ ,  ${}^3P_1 \rightarrow {}^3H_4$  and  ${}^3P_0 \rightarrow {}^3H_4$ , respectively. The excitation spectra indicate that the  $\text{SrMoO}_4:\text{Pr}$  thin films can be excited efficiently by the UV radiation. Moreover, the  $\text{SrMoO}_4:\text{Pr}$  thin films can be excited by the blue light but it is faint.

Fig. 5c shows the emission spectra of the  $\text{SrMoO}_4:\text{Pr}_{0.04}$  (2–12 layers) samples. All the six samples exhibit similar luminescence emission behavior with no significant change in peak position, but the emission intensities are mutative. The  $\text{Pr}^{3+}$  doped  $\text{SrMoO}_4$  films show deep red emission which can attribute to the strongest peak at 646 nm and the three shoulder peaks located at 603 nm, 618 nm and 730 nm. The emission peaks corresponding to  ${}^1D_2 \rightarrow {}^3H_4$  (602 nm),  ${}^3P_0 \rightarrow {}^3H_6$  (618 nm),  ${}^3P_0 \rightarrow {}^3F_2$  (646 nm),  ${}^3P_0 \rightarrow {}^3F_3$  (730 nm) ascribe to  $f \rightarrow f$  transitions of  $\text{Pr}^{3+}$  [28]. As shown in Fig. 5b, the absorption intensity of  $\text{Pr}^{3+}$  is weaker comparing with  $\text{MoO}_4^{2-}$  groups, so the characteristic emission of the doped rare earth ions ( $\text{Pr}^{3+}$ ) can be attributed to an efficient energy transfer from the  $\text{MoO}_4^{2-}$  groups to  $\text{Pr}^{3+}$  ions [7,35]. The relative intensity of the visible emission spectra increases gradually with the increase of layers. This reaches to 8 layers, the emission increase is less apparent when the number of layers keeps on increasing.

Fig. 5d displays the excitation spectra recorded at 1037 nm. The only broad excitation peak between 230 nm and 270 nm is assigned to charge transfer from the  $\text{SrMoO}_4$  host matrix. The NIR emissions spectra were obtained under excitation with 260 nm, as show in Fig. 5e. The strongest intensity of NIR emission peak at 1037 nm belong to the  $\text{Pr}^{3+}: {}^1G_4(\Gamma_{3,4}) \rightarrow {}^3H_4(\Gamma_1)$  transition. In addition, the peaks at 818 nm, 861 nm, 981 nm, 1001 nm, 1021 nm 1456 nm and 1503 nm are ascribed to  ${}^1D_2(\Gamma_{3,4}) \rightarrow {}^3F_2(\Gamma_{3,4})$ ,

${}^1D_2(\Gamma_{3,4}) \rightarrow {}^3F_2(\Gamma_{3,4})$ ,  ${}^1G_4(\Gamma_{5,6}) \rightarrow {}^3H_4(\Gamma_{5,6})$ ,  ${}^1G_4(\Gamma_{3,4}) \rightarrow {}^3H_4(\Gamma_1)$ ,  ${}^1G_4(\Gamma_1) \rightarrow {}^3H_4(\Gamma_{3,4})$ ,  ${}^3F_3(\Gamma_{3,4}) \rightarrow {}^3H_4(\Gamma_2)$  and  ${}^3F_3(\Gamma_{3,4}) \rightarrow {}^3H_4(\Gamma_2)$  transitions. The variation tendencies of visible emission intensity and NIR emission intensity with various layers are illustrated in Fig. 5f. The emission intensities ascend with layers increasing, but the intensities will no longer be enhanced when the process of spin coating repeated 8 times. The gradual saturation tendency can be attributed to the restriction of grain growth. The emission intensity can be enhanced with the grain size. However, as the layer number further increasing, the grain growth becomes more and more difficult due to the mutual extrusion between the grains.

According to the above initial luminescent results of various layers of films, we selected the fixed eight-layer thin films to investigate the controllable growth process and the relationship between  $\text{Pr}^{3+}$  concentration and the luminescent intensity of the thin film. The visible and NIR emission spectra of  $\text{Pr}^{3+}$ -doped  $\text{SrMoO}_4$  thin films with the increasing  $\text{Pr}^{3+}$  concentration from 1 to 6 mol % is shown in Fig. 6. As depicted in Fig. 6a, the emission intensity varies with doping concentration, and the maximal emission occurs at  $c = 4$  mol%. Furthermore, the chromaticity coordinates of the  $\text{SrMoO}_4:\text{Pr}_{0.04}$  has been calculated via the 1931 CIE (Commission International de l'Eclairage). Their coordinates are  $x = 0.6556$ ,  $y = 0.3468$ , marked as a star in Fig. 6b. The recorded data demonstrates that the  $\text{SrMoO}_4:\text{Pr}$  thin film has a red emission and the color trends to deep red. Interestingly, the same phenomenon also occurs in NIR emission spectra, as shown in Fig. 6c. The integrated visible emission intensities and NIR emission intensities of  $\text{SrMoO}_4:\text{Pr}$  thin films as a function of doping content are illustrated in Fig. 6d. We can intuitively see that the emission intensity increased gradually with increasing  $\text{Pr}^{3+}$  concentration. However, a decline occurs miraculously when this reaches a maximum at  $c = 4$  mol%. The unusual decline can be

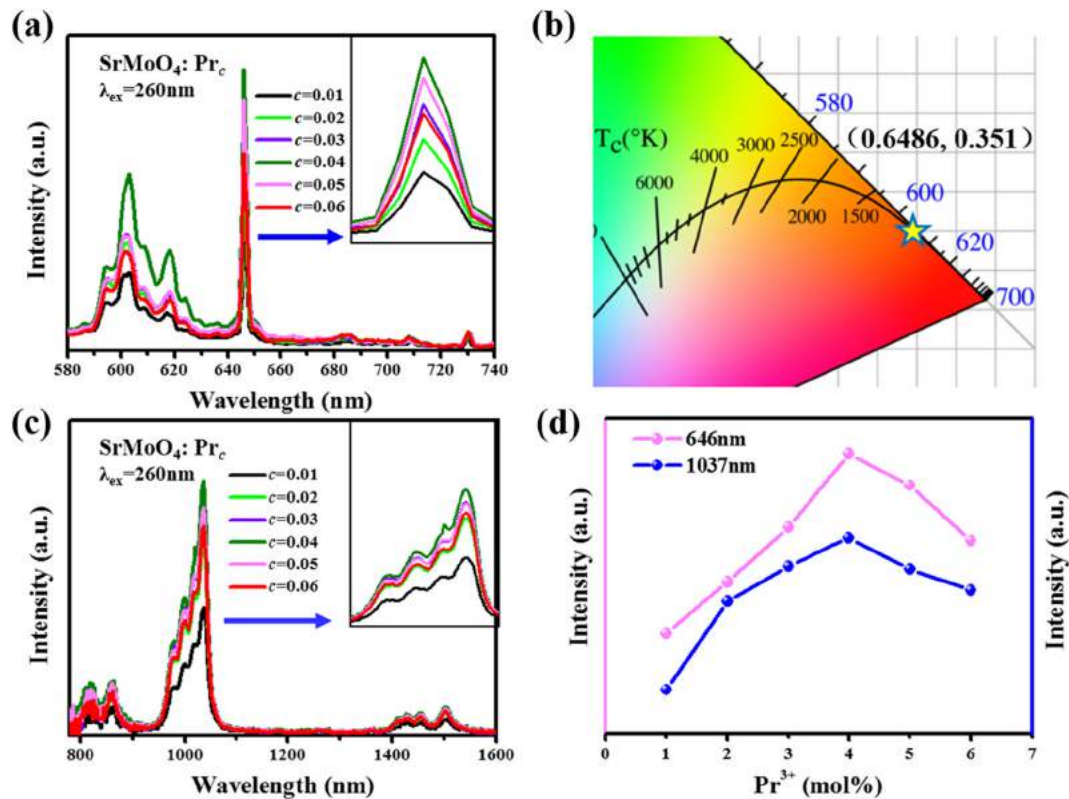


Fig. 6. The photoluminescence properties of as-prepared thin films with various doping concentrations. (a) Emission spectra of  $\text{SrMoO}_4:\text{Pr}_c$  ( $c = 0.01\text{--}0.06$ ) thin films under excitation at 260 nm. (b) CIE diagram for  $\text{SrMoO}_4:\text{Pr}_c$  ( $c = 0.04$ ) thin film. (c) NIR emission spectra of  $\text{SrMoO}_4:\text{Pr}_c$  ( $c = 0.01\text{--}0.06$ ) thin films under excitation at 260 nm. (d) The integrated visible and NIR emission intensity of  $\text{SrMoO}_4:\text{Pr}_c$  ( $c = 0.01\text{--}0.06$ ) thin films under excitation at 260 nm.

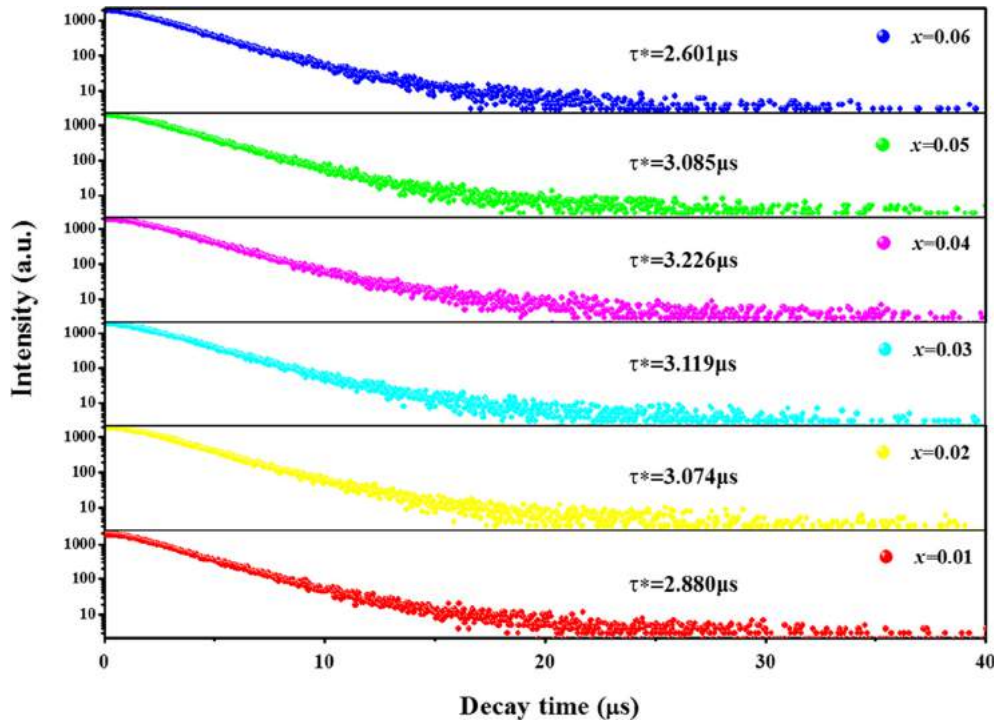


Fig. 7. PL decay profiles of SrMoO<sub>4</sub>: Pr<sub>c</sub> ( $c = 0.01$ – $0.06$ ) under an excitation wavelength of 265 nm and emission wavelength of 646 nm.

attribute to the concentration quenching, the chief reasons are non-radiation transition and cross-relaxation. With the increase of the doped Pr<sup>3+</sup> ions, the distance among Pr<sup>3+</sup> ions is shortened, non-radiation transition occurs with a greater likelihood. Additionally, some cross-relaxation such as  ${}^3P_0 + {}^3H_4 \rightarrow {}^1D_2 + {}^3H_6$  and  ${}^1D_2 + {}^3H_4 \rightarrow {}^3F_4 + {}^1G_4$  can cause the emission quenching. Therefore, the luminescence performance is at its best when the doping concentration increases to 4 mol%.

In order to verify the energy transfer from host material to doping ions, luminescence decay curves of SrMoO<sub>4</sub>: Pr<sub>c</sub> ( $c = 0.01$ – $0.06$ ) thin films excited at 265 nm are illustrated in Fig. 7. All the decay curves display the double exponential behavior according to the following equation [36]:

$$I(t) = A_1 e^{-t/\tau_1} + A_2 e^{-t/\tau_2} \quad (1)$$

where  $I(t)$  is the luminescence intensity,  $A_1$  and  $A_2$  are constant;  $t$  is the time;  $\tau_1$  and  $\tau_2$  are fast and slow lifetimes. The average decay time ( $\tau^*$ ) of the  ${}^3P_0 \rightarrow {}^3F_2$  can be defined by the equation as follows [36]:

$$\tau^* = (A_1 \tau_1^2 + A_2 \tau_2^2) / (A_1 \tau_1 + A_2 \tau_2) \quad (2)$$

The lifetime value of  $\tau_1$ ,  $\tau_2$ ,  $A_1$ ,  $A_2$ ,  $\tau^*$  and  $R^2$  are summarized in Table 1. The average decay times were calculated using the equation and considered to be 2.88  $\mu$ s, 3.074  $\mu$ s, 3.119  $\mu$ s, 3.226  $\mu$ s, 3.085  $\mu$ s and 2.601  $\mu$ s, respectively. It can be clearly seen that the lifetimes obviously increase as the Pr<sup>3+</sup> doping concentration increases, but

the unexpected downturn occur when the Pr<sup>3+</sup> concentration range from 5% to 6%. At low concentration, the smaller interaction between two adjacent Pr<sup>3+</sup> ions cannot cause the increased non-radiative transition. However, as a result of reduced distance, this kind of naturally augmented interaction leads to an increased possibility of energy transfer to killer sites, resulting in the shortened lifetimes. Both the non-radiative transition mode and the transfer speed are inevitably affected by the increased Pr<sup>3+</sup> concentration. This variation tendency is consistent with the luminescence intensity of SrMoO<sub>4</sub>: Pr<sub>c</sub> ( $c = 0.01$ – $0.06$ ). In order to accurately evaluate the luminescence efficiency of the samples, an integrating sphere system were used to collect information and the quantum yields were obtained by the following equation [37]

$$QY = \frac{L_{\text{sample}}}{E_{\text{reference}} - E_{\text{sample}}} \quad (3)$$

where QY,  $L_{\text{sample}}$ ,  $E_{\text{reference}}$ ,  $E_{\text{sample}}$  are the quantum yield, the emission intensity, the excitation intensity of the reference sample and the test sample, respectively. The quantum yield values of the thin films with a range of doping concentrations are displayed in Table 1. Enhanced radiative transition and suppressed non-radiative transition are the key to enhance quantum yield. Not coincidentally, the quantum yield shows a similar tendency with the decay times, and the maximum quantum yield is as high as 86.21% when the Pr<sup>3+</sup> ions concentration is 4%.

Table 1

Fast decay lifetime ( $\tau_1$ ), slow decay lifetimes ( $\tau_2$ ), average lifetime ( $\tau$ -) and quantum efficiency (QY) of SrMoO<sub>4</sub>: Pr<sub>c</sub> ( $c = 0.01$ – $0.06$ ) thin films.

Sample	$\tau_1$ (ns)	$A_1$	$\tau_2$ (ns)	$A_2$	$\tau$ - (ns)	$x^2$	QY%
$c = 0.01$	2579	2281	13,191	13	2880	1.083	17.84
$c = 0.02$	2691	2294	19,982	7	3074	1.214	30.02
$c = 0.03$	2677	2305	20,096	8	3119	1.269	44.60
$c = 0.04$	2786	2427	22,298	7	3226	1.602	86.21
$c = 0.05$	2676	2357	19,580	8	3085	1.307	50.83
$c = 0.06$	2602	2376	15,953	8	2601	1.157	46.79

#### 4. Conclusion

In summary, a series of Pr<sup>3+</sup> ions doped SrMoO<sub>4</sub> thin films were mounted on the common quartz substrates by a facile and versatile polymer-assisted deposition (PAD) method. By virtue of the strong chelation between water-soluble polymer and metal ions, the bonded metal ions can be evenly distributed in the precursor solution, the controllable nucleation and growth of SrMoO<sub>4</sub>: Pr thin films can be realized effectively. Compared with previous reports, the grains of prepared SrMoO<sub>4</sub>: Pr thin films are more uniform and dense by slowly releasing the interfacial strain [5,38]. Under the excitation of UV light, the SrMoO<sub>4</sub>: Pr thin films exhibit deep red and NIR emission and their emission intensities can be flexibly adjusted via regulating the number of deposition layers and Pr<sup>3+</sup> ions concentrations. Additionally, the thin film showed a maximum emission intensity at c = 4 mol% with an overwhelmingly high photoluminescence quantum yield of 86.21%. The prospective SrMoO<sub>4</sub>: Pr luminescent films with visible and NIR emission properties will have potential application in UV excited LED, telecommunications, optical communications and drug delivery. But above all, this research provides a new clue for the preparation of other diverse fluorescent thin films.

#### Acknowledgements

This work was supported by the National Natural Science Foundation of China (No. 51602265), the Scientific and Technological Projects for Distinguished Young Scholars of Sichuan Province (No. 2015JQ0013), the Fundamental Research Funds for the Central Universities of China (A0920502051408-10, ZYGX2009Z0001 and A0920502051619-72), China Postdoctoral Science Foundation (2016M592692).

#### References

- J.C. Sczancoski, M.D.R. Bomio, L.S. Cavalcante, M.R. Joya, P.S. Pizani, J.A. Varela, E. Longo, M.S. Li, J. Andres, Morphology and blue photoluminescence emission of PbMoO<sub>4</sub> processed in conventional hydrothermal, *J. Phys. Chem. C* 113 (2009) 5812–5822.
- X. Tang, X. Zhu, J. Dai, J. Yang, L. Hu, L. Chen, X. Zhu, X. Li, H. Jiang, R. Zhang, Y. Sun, c-Axis oriented SrMoO<sub>4</sub> thin films by chemical solution deposition: self-assembled orientation, grain growth and photoluminescence properties, *Acta Mater.* 65 (2014) 287–294.
- Y.N. Zhu, G.H. Zheng, Z.X. Dai, L.Y. Zhang, J.J. Mu, Core-shell structure and luminescence of SrMoO<sub>4</sub>: Eu<sup>3+</sup> (10%) phosphors, *J. Mater. Sci. Technol.* 32 (2016) 1361–1371.
- N. Niu, P. Yang, W. Wang, F. He, S. Gai, D. Wang, J. Lin, Solvothermal synthesis of SrMoO<sub>4</sub>: Ln (Ln = Eu<sup>3+</sup>, Tb<sup>3+</sup>, Dy<sup>3+</sup>) nanoparticles and its photoluminescence properties at room temperature, *Mater. Res. Bull.* 46 (2011) 333–339.
- D. Rangappa, T. Fujiwara, T. Watanabe, M. Yoshimura, Fabrication of AMO<sub>4</sub> (A = Ba, Sr, Ca M = Mo, W) films on M substrate by solution reaction assisted ball rotation, *J. Electroceram.* 17 (2006) 853–860.
- C. Shivakumara, R. Saraf, Eu<sup>3+</sup>-activated SrMoO<sub>4</sub> phosphors for white LEDs applications: synthesis and structural characterization, *Opt. Mater.* 42 (2015) 178–186.
- Y. Tian, B. Chen, B. Tian, R. Hua, J. Sun, L. Cheng, H. Zhong, X. Li, J. Zhang, Y. Zheng, T. Yu, L. Huang, Q. Meng, Concentration-dependent luminescence and energy transfer of flower-like Y<sub>2</sub>(MoO<sub>4</sub>)<sub>3</sub>: Dy<sup>3+</sup> phosphor, *J. Alloys Compd.* 509 (2011) 6096–6101.
- E.E. Dunaeva, L.I. Ivleva, M.E. Doroshenko, P.G. Zverev, V.V. Osiko, SrMoO<sub>4</sub>: Pr<sup>3+</sup> single crystals: growth and properties, *Dokl. Phys.* 60 (2015) 122–126.
- J. Cao, Y. Wang, X. Ma, J. Li, Z. Zhu, Z. You, F. Yang, C. Sun, T. Cao, Y. Ji, C. Tu, Spectroscopic properties of Pr<sup>3+</sup>: SrMoO<sub>4</sub> crystal, *J. Alloys Compd.* 509 (2011) 185–189.
- W. Xia, S. Xiao, X. Yang, X. Jin, Quantum cutting and tunable luminescence properties in Pr<sup>3+</sup>/Sm<sup>3+</sup>, Yb<sup>3+</sup> Co-doped SrMoO<sub>4</sub> powders, *Mater. Res. Bull.* 89 (2017) 5–10.
- X. Teng, Y. Zhu, W. Wei, S. Wang, J. Huang, R. Naccache, W. Hu, A.I.Y. Tok, Y. Han, Q. Zhang, Q. Fan, W. Huang, J.A. Capobianco, L. Huang, Lanthanide-doped Na<sub>x</sub>ScF<sub>3-x</sub> nanocrystals: crystal structure evolution and multicolor tuning, *J. Am. Chem. Soc.* 134 (2012) 8340–8343.
- F. Wang, X. Liu, Upconversion multicolor fine-tuning: visible to near-infrared emission from lanthanide-doped NaYF<sub>4</sub> nanoparticles, *J. Am. Chem. Soc.* 130 (2008) 5642–5643.
- V. Caratto, F. Locardi, G.A. Costa, R. Masini, M. Fasoli, L. Panzeri, M. Martini, E. Bottinelli, E. Gianotti, I. Miletto, NIR persistent luminescence of lanthanide ion-doped rare-earth oxycarbonates: the effect of dopants, *ACS Appl. Mater. Interfaces* 6 (2014) 17346–17351.
- A. Mech, A. Monguzzi, F. Meinardi, J. Mezyk, G. Macchi, R. Tubino, Sensitized NIR erbium(III) emission in confined geometries: a new strategy for light emitters in telecom applications, *J. Am. Chem. Soc.* 132 (2010) 4574.
- X. Liu, Y. Fan, S. Chen, M. Gu, C. Ni, B. Liu, S. Huang, Luminescence properties of Li-codoped Lu<sub>2</sub>SiO<sub>5</sub>: Ce thin-film phosphors prepared by sol-gel processing, *Mater. Res. Bull.* 48 (2013) 2370–2374.
- H. Hao, H. Lu, R. Meng, Z. Nie, G. Ao, Y. Song, Y. Wang, X. Zhang, Thermometry via Au island-enhanced luminescence of Er<sup>3+</sup>/Yb<sup>3+</sup> co-doped Gd<sub>2</sub>(MoO<sub>4</sub>)<sub>3</sub> thin films, *J. Alloys Compd.* 695 (2017) 2065–2071.
- X. Fu, H. Yamada, K. Nishikubo, H. Zhang, C.N. Xu, Preparation and characterization of fiber-textured SrAl<sub>2</sub>O<sub>4</sub>: Eu films grown using a homo-buffer layer, *J. Cryst. Growth* 310 (2008) 2885–2889.
- X. Liu, X. Zhang, Z. Zhou, Preparation and luminescence properties of patterned SOG/Sr<sub>2</sub>MgSi<sub>2</sub>O<sub>7</sub>: Eu<sup>2+</sup>, Dy<sup>3+</sup> long-persistent luminescence composite thin films by one-step photolithography, *Mater. Res. Bull.* 79 (2016) 84–89.
- P.D. Nsimama, O.M. Ntwaeaborwa, H.C. Swart, The effect of different gas atmospheres on luminescent properties of pulsed laser ablated SrAl<sub>2</sub>O<sub>4</sub>: Eu<sup>2+</sup>, Dy<sup>3+</sup> thin films, *J. Lumin.* 131 (2011) 119–125.
- F. Chun, B. Zhang, H. Su, H. Osman, W. Deng, W. Deng, H. Zhang, W. Yang, Preparation and luminescent properties of self-organized broccoli-like SrMoO<sub>4</sub>: Pr<sup>3+</sup> superparticles, *J. Lumin.* 190 (2017) 69–75.
- G. Zou, H. Luo, F. Ronning, B. Sun, T.M. McCleskey, A.K. Burrell, E. Bauer, Q.X. Jia, Facile chemical solution deposition of high-mobility epitaxial germanium films on silicon, *Angew. Chem., Int. Ed.* 49 (2010) 1782–1785.
- J.L. MacManus-Driscoll, S.R. Foltyn, Q.X. Jia, H. Wang, A. Serquis, B. Maiorov, L. Civale, Y. Lin, M.E. Hawley, M.P. Maley, D.E. Peterson, Systematic enhancement of in-field critical current density with rare-earth ion size variance in superconducting rare-earth barium cuprate films, *Appl. Phys. Lett.* 84 (2004) 5329–5331.
- T.M. McCleskey, P. Shi, E. Bauer, M.J. Highland, J.A. Eastman, Z.X. Bi, P.H. Fuoss, P.M. Baldo, W. Ren, B.L. Scott, A.K. Burrell, Q.X. Jia, Nucleation and growth of epitaxial metal-oxide films based on polymer-assisted deposition, *Chem. Soc. Rev.* 43 (2014) 2141–2146.
- H. Luo, H. Wang, Z. Bi, G. Zou, T.M. McCleskey, A.K. Burrell, E. Bauer, M.E. Hawley, Y. Wang, Q. Jia, Highly conductive films of layered ternary transition-metal nitrides, *Angew. Chem., Int. Ed.* 48 (2009) 1490–1493.
- Y. Zhang, N. Haberkorn, F. Ronning, H. Wang, N.A. Mara, M. Zhuo, L. Chen, J.H. Lee, K.J. Blackmore, E. Bauer, A.K. Burrell, T.M. McCleskey, M.E. Hawley, R.K. Schulze, L. Civale, T. Tajima, Q. Jia, Epitaxial superconducting delta-MoN films grown by a chemical solution method, *J. Am. Chem. Soc.* 133 (2011) 20735–20737.
- G. Zou, H. Wang, N. Mara, H. Luo, N. Li, Z. Di, E. Bauer, Y. Wang, T. McCleskey, A. Burrell, X. Zhang, M. Nastasi, Q. Jia, Chemical solution deposition of epitaxial carbide films, *J. Am. Chem. Soc.* 132 (2010) 2516–2517.
- G.F. Zou, J. Zhao, H.M. Luo, T.M. McCleskey, A.K. Burrell, Q.X. Jia, Polymer-assisted-deposition: a chemical solution route for a wide range of materials, *Chem. Soc. Rev.* 42 (2013) 439–449.
- R.B. Mos, T.J. Petrisor, M. Nasui, A. Mesaros, M.S. Gabor, M. Senila, E. Ware, L. Ciontea, T. Petrisor, Epitaxial La<sub>0.7</sub>Sr<sub>0.3</sub>MnO<sub>3</sub> nanostructures obtained by polymer-assisted surface decoration (PASD), *Mater. Lett.* 171 (2016) 281–284.
- X. Feng, W. Feng, K. Wang, Experimental and theoretical spectroscopic study of praseodymium(III) doped strontium aluminate phosphors, *J. Alloys Compd.* 628 (2015) 343–346.
- A. Pérez-Rivero, M. Cabero, M. Varela, R. Ramírez-Jiménez, F. Mompean, J. Santamaría, J. Martínez, C. Prieto, Thermoelectric functionality of Ca<sub>3</sub>Co<sub>4</sub>O<sub>9</sub>, epitaxial thin films on yttria-stabilized zirconia crystalline substrate, *J. Alloys Compd.* 710 (2017) 151–158.
- H. Luo, M. Jain, T. McCleskey, E. Bauer, A. Burrell, Q. Jia, Optical and structural properties of single phase epitaxial p-type transparent oxide thin films, *Adv. Mater.* 19 (2010) 3604–3607.
- Y. Lin, H. Wang, M.E. Hawley, S.R. Foltyn, Q.X. Jia, G.E. Collis, A.K. Burrell, T.M. McCleskey, Epitaxial growth of Eu<sub>2</sub>O<sub>3</sub> thin films on LaAlO<sub>3</sub> substrates by polymer-assisted deposition, *Appl. Phys. Lett.* 85 (2004) 3426–3428.
- T. Sameshima, M. Hara, S. Usui, Measuring the temperature of a quartz substrate during and after the pulsed laser-induced crystallization of a-Si:H, *Jpn. J. Appl. Phys.* 28 (2014) L2131–L2133.
- Q.X. Jia, T.M. McCleskey, A.K. Burrell, Y. Lin, G.E. Collis, H. Wang, A.D.Q. Li, S.R. Foltyn, Polymer-assisted deposition of metal-oxide films, *Nat. Mater.* 3 (2004) 529–532.
- P. Yang, C. Li, W. Wang, Z. Quan, S. Gai, J. Lin, Uniform AMO<sub>4</sub>: Ln (A = Sr<sup>2+</sup>, Ba<sup>2+</sup>; Ln = Eu<sup>3+</sup>, Tb<sup>3+</sup>) submicron particles: solvothermal synthesis and luminescent properties, *J. Solid State Chem.* 182 (2009) 2510–2520.
- S.P. Lee, S.D. Liu, T.S. Chan, T.M. Chen, Synthesis and luminescence properties of novel Ce<sup>3+</sup> and Eu<sup>2+</sup> doped lanthanum bromothiosilicate La<sub>3</sub>Br(Si<sub>3</sub>S<sub>4</sub>)<sub>2</sub> phosphors for white LEDs, *ACS Appl. Mater. Interfaces* 8 (2016) 9218–9223.
- J.C. Boyer, F.C. van Veggle, Absolute quantum yield measurements of colloidal NaYF<sub>4</sub>: Er<sup>3+</sup>, Yb<sup>3+</sup> upconverting nanoparticles, *Nanoscale* 2 (2010) 1417–1419.
- D.Y. Kim, J.S. Kim, B.H. Park, J.K. Lee, J.H. Kim, J.H. Lee, J. Chang, H.J. Kim, I. Kim, Y.D. Park, SrFeO<sub>3</sub> nanoparticles-dispersed SrMoO<sub>4</sub> insulating thin films deposited from Sr<sub>2</sub>FeMoO<sub>6</sub> target in oxygen atmosphere, *Appl. Phys. Lett.* 84 (2004) 5037–5039.